ASGE Vol. 06 (03), pp. 65-95, 2022

Egyptian Knowledge Bank

International Journal of Advances in Structural and Geotechnical Engineering

https://asge.journals.ekb.eg/

Print ISSN 2785-9509 *Online ISSN 2812-5142*

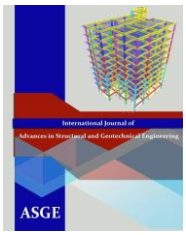

Finite Element Formulation of Timoshenko Non-Prismatic Beam-Column Element for Static and Dynamic Analysis of Wind Turbine Towers

Mohamed Mohamedien [1], Ezzaat Sallam [2], Omar El Gendy [3]

[1]*Professor, Faculty of Engineering, Suez Canal University, Egypt*
[2] *Teacher, Faculty of Engineering, Port Said University, Egypt*
[3]*Teacher Assistant, Faculty of Engineering, Suez Canal University, Egypt*

ABSTRACT

In this paper, a numerical formulation is carried out to produce stiffness and consistent mass matrices for two-nodal non-prismatic Timoshenko beam-column elements. The proposed solution is based on the exact shape functions and their derivatives describing the non-uniformity of the element properties. To illustrate the variations in section properties along the tapered element length, the mechanical properties are presented as power functions with tapering indices. The model is applicable for elements with different solid and hollow cross-sections. The Proposed formulation is embedded into a visual basic code to carry out the analysis accompanied with many examples for validating its accuracy and efficiency. The model results are compared with those of commercial software and cited references which showed high accurate results with a small number of elements. Finally, a numerical study using the proposed solution was performed on a wind turbine tower to carry out a free vibration and linear stability analysis.

Keywords: Finite Element; Timoshenko Beam; Non-prismatic element; Beam-Column element, Free vibration; Linear Stability.

INTRODUCTION

Wind energy plays an important role in sustainability-focused policies and experiences the fastest growth rate of renewable energy sources. Although the cost of wind energy has decreased rapidly in the last decade, more cost reduction can be achieved. Improving the accuracy and efficiency of the analysis process used in the design can lead to more economical designs. The numerical structural modelling of the wind turbine tower is an essential part for the wind turbine design. The tower can be modelled as 3D structure, shell or beam-column. Using 3D structure or shell models need large number of elements and nodes that leads to large number of unknowns. The analysis process can be somewhat complicated and needs more time and effort to be reached. Using beam-column element can be more efficient if the model used is suitable and takes into account the best simulation for the behavior of this type of structures. There are many commercial programs that incorporate mathematical models to represent the beams. Most of these models consider a constant cross section throughout the element. Therefore, when modeling a wind turbine tower using these models, we will need a large number of elements to obtain high-precision results. To overcome this obstacle, a mathematical model for the beam-column element was derived based on exact shape functions for deformations caused by axial forces, flexure, and torsion. The model proposed in this study is based on the Timoshenko beam model, which takes into account the transverse shear deformations. Linear and geometrical stiffness matrices and consistent mass matrix were derived based on the previous principles.

To model tapered members, two simplified approaches are widely used to achieve the analysis. The stepped-element and the approximated-stiffness methods. The first method is present in all commercial programs, and it is based on dividing single tapered element into an appropriate number of constant elements. Practically, this method requires a large number of sub-elements to represent a single tapered element, which increases the efforts of the calculation process. The second method is to simplify the variations of flexural rigidities along the element by representing it by linear, parabolic or cubic functions. The second method has been used by many researches such as Valipour and Bradford (2012), Rezaiee-Pajand et al. (2016). The accuracy of the previous method is sometimes questionable because it is based on empirical assumptions. Other methods to represent non-prismatic elements can found in Attarnejad etc al. (2010) and Tudjono etc al. (2017) and Bai etc al. (2018). Attarnejad etc al. (2010) presented basic displacement functions (BDFs) by means of power series method for free vibration analysis of tapered Timoshenko beams. while Tudjono etc al. (2017) derived the stiffness and consistent mass equations of Timoshenko non-uniform and non-homogeneous beams. Tudjono etc al. (2017) used the Gaussian quadrature integration scheme to get the exact shape functions and then finding the stiffness and consistent mass matrices. Bai etc al. (2018) derived beam-column formulations based on shape functions established upon the local axes by extracting the rigid-body movements for simplifying mathematical expressions.

Most of the wind turbine towers are made as truncated hollow cones with diameters varying linearly, parabolically or cubically. These towers can be modelled as tapered beam elements with a circular hollow cross section. Many researches such as Arany etc al. (2015 and 2016), Alamouti etc al. (2017), Bouzid etc al. (2017), Álamo, G. etc al. (2018) and Yung-Yen Ko (2020) used beam elements to simulate wind turbine towers especially offshore wind turbines resting on monopiles .

The present FE model could be considered as closed forms for stiffness and consistent mass matrices. The proposed model is apple to analyze Timoshenko tapered beams with different cross section types and tapering ratios with high accuracy and low number of finite elements. Timoshenko beam refers to beams considering transverse shear effect in analysis, which is differ from Euler-Bernoulli beam that neglect the transverse shear effect. Element linear stiffness, consistent mass and geometric matrices are developed based on exact shape functions of the deformations, which would give more accurate results and a smaller number of elements.

ASSUMPTIONS AND DEFINITIONS

The following assumptions are made in the present study to simplify the derivation of the tapered element:

- Strains are small.
- Material is homogeneous, isotropic and in elastic state.
- Only pure torsion is considered; warping is not considered in the proposed model.
- Shear coefficient of hollow sections is constant along the element.
- Thickness of hollow sections are constant along the element.

PROPERTIES OF A TAPERED ELEMENT

By defining the geometrical and mechanical properties, the present model is applicable for different cross sections, but this paper will focus on hollow circular sections.
For a tapered beam element with a circular hollow cross section, the section properties vary from the thin end to the thick end as following:

$$D(x) = D_i\left(1+r_A\frac{x}{L}\right) \tag{1}$$

$$A(x) = \frac{\pi}{4}\left(D(x)^2 - D'(x)^2\right) = A_i\left(1+r_A\frac{x}{L}\right)^{\Gamma} \tag{2}$$

$$I(x) = \frac{\pi}{64}\left(D(x)^4 - D'(x)^4\right) = I_i\left(1+r_A\frac{x}{L}\right)^{\bar{\Gamma}} \tag{3}$$

$$J(x) = I_p(x) = 2I(x) = I_{pi}\left(1+r_A\frac{x}{L}\right)^{\Gamma_p} = J_i\left(1+r_A\frac{x}{L}\right)^{\Gamma_J} \tag{4}$$

$$\kappa = \frac{6(1+\nu)\left(1+\left(\frac{D'}{D}\right)^2\right)^2}{(7+6\nu)\left(1+\left(\frac{D'}{D}\right)^2\right)^2 + (20+12\nu)\left(\frac{D'}{D}\right)^2} \tag{5}$$

where
D: the tapered geometry parameter (diameter of circular sections, height or breadth in other sections).
L, A, I, J: are the length, area, second moment of area and torsional constant, respectively.
i, j: denotes the right (thin) and left (thick) ends of the element, respectively.
n: a superscript denotes the power of tapering, it equals 1 for linear, 2 for parabolic, 3 for cubic.
κ: is the shear factor for circular hollow section which is nearly constant along the element.
b: is the ratio between the inner and outer diameters of the hollow circular section.
r_D, r_A are the tapering ratio of diameter and area respectively, which are given by:

$$r_D = \left(\frac{D_j}{D_i}\right) - 1 \tag{6}$$

$$r_A = \left(\frac{A_j}{A_i}\right) - 1 \tag{7}$$

Γ: is the tapering index of area, it equals to 1 for the following section types:

- Tapered hollow circular sections.
- Tapered hollow rectangular sections.
- Tapered solid rectangular sections with variable depth and constant breadth or vice versa.

and, it equals to 2 for the following section types:

- Tapered solid circular sections.
- Tapered solid rectangular sections with depth and breadth varying with the same ratio.

other tapering indices can be calculated as:

$$\bar{\Gamma} = \frac{\ln\left(I_{sj}/I_{si}\right)}{\ln(1+r_A)},\ s=z \text{ or } y \tag{8}$$

$$\Gamma_p = \frac{\ln\left(I_{pj}/I_{pi}\right)}{\ln(1+r_A)} \tag{9}$$

$$\Gamma_J = \frac{\ln(J_j/J_i)}{\ln(1+r_A)} \tag{10}$$

MATHEMATICAL MODEL

In this section, a *Timoshenko* tapered frame element stiffness, consistent mass and geometric stiffness matrices are derived based on exact shape functions of the deformations, which would give more accurate results and a smaller number of elements. *Timoshenko* beam refers to beams considering transverse shear and rotational bending effects in analysis, which is differ from *Euler-Bernoulli* beam that neglect these effects and consider the cross sections remain normal to the neutral axis after deformation.

Element linear stiffness matrix

The governing differential equations for a *Timoshenko* tapered frame element considering the superposition of axial, torsion and biaxial bending effects can be found in different references as *Logan* (2012), *McGuire etc al*. (1999), *Tudjono etc al* (2017) and others as:

$$\frac{d}{dx}\left(EA(x)\frac{du}{dx}\right)=0 \tag{11}$$

$$\frac{d}{dx}\left(GJ(x)\frac{d\theta_x}{dx}\right)=0 \tag{12}$$

$$\frac{d^2}{dx^2}\left(EI_z(x)\frac{d\theta_z}{dx}\right)=0 \tag{13}$$

$$\frac{d}{dx}\left(EI_z(x)\frac{d\theta_z}{dx}\right)+\kappa GA(x)\left(\frac{dv}{dx}-\theta_z\right)=0 \tag{14}$$

$$\frac{d^2}{dx^2}\left(EI_y(x)\frac{d\theta_y}{dx}\right)=0 \tag{15}$$

$$\frac{d}{dx}\left(EI_y(x)\frac{d\theta_y}{dx}\right)+\kappa GA(x)\left(\frac{dw}{dx}-\theta_y\right)=0 \tag{16}$$

where:
E: is the modulus of elasticity.
G: is the shear modulus of elasticity.
v: is *Poisson's* ratio.
These equations present six degree of freedoms per node; three rotations (θ_x, θ_y, θ_z) and three translations (u, v, w). Solving the previous differential equations lead to get the displacements equations distributed according to exact shape functions and depending on the two ends displacements. By solving equation (11), the exact shape functions and there first order derivatives of the axial displacement can be performed as:

$$\{u(x)\}= [1-\xi_A \quad \xi_A] \begin{Bmatrix} u_i \\ u_j \end{Bmatrix} = [N_{u1} \quad N_{u2}] \begin{Bmatrix} u_i \\ u_j \end{Bmatrix} = [N_u] \begin{Bmatrix} u_i \\ u_j \end{Bmatrix} \tag{17}$$

$$\left\{\frac{du}{dx}\right\}= [-\xi'_A \quad \xi'_A] \begin{Bmatrix} u_i \\ u_j \end{Bmatrix} = [N'_{u1} \quad N'_{u2}] \begin{Bmatrix} u_i \\ u_j \end{Bmatrix} = [N'_u] \begin{Bmatrix} u_i \\ u_j \end{Bmatrix} \tag{18}$$

In the same way, the exact shape functions and there first order derivatives of the torsional angle can be performed by solving equation (12) as:

$$\{\theta_x(x)\}= [1-\xi_T \quad \xi_T] \begin{Bmatrix} \theta_{xi} \\ \theta_{xj} \end{Bmatrix} = [N_{\theta x1} \quad N_{\theta x2}] \begin{Bmatrix} \theta_{xi} \\ \theta_{xj} \end{Bmatrix} = [N_{\theta x}] \begin{Bmatrix} \theta_{xi} \\ \theta_{xj} \end{Bmatrix} \tag{19}$$

$$\left\{\frac{d\theta_x}{dx}\right\}= [-\xi'_T \quad \xi'_T] \begin{Bmatrix} \theta_{xi} \\ \theta_{xj} \end{Bmatrix} = [N'_{\theta x1} \quad N'_{\theta x2}] \begin{Bmatrix} \theta_{xi} \\ \theta_{xj} \end{Bmatrix} = [N'_{\theta x}] \begin{Bmatrix} \theta_{xi} \\ \theta_{xj} \end{Bmatrix} \tag{20}$$

In the same way, the exact shape functions and there first order derivatives of the bending about *z* rotations and displacements can be performed by solving the two equations (13) and (14) as:

$$\{\theta_z(x)\} = [N_{\theta z1} \quad N_{\theta z2} \quad N_{\theta z3} \quad N_{\theta z4}] \begin{Bmatrix} v_i \\ \theta_{zi} \\ v_j \\ \theta_{zj} \end{Bmatrix} = [N_{\theta z}] \begin{Bmatrix} v_i \\ \theta_{zi} \\ v_j \\ \theta_{zj} \end{Bmatrix} \tag{21}$$

$$\left\{\frac{d\theta_z}{dx}\right\} = [N'_{\theta z1} \quad N'_{\theta z2} \quad N'_{\theta z3} \quad N'_{\theta z4}] \begin{Bmatrix} v_i \\ \theta_{zi} \\ v_j \\ \theta_{zj} \end{Bmatrix} = [N'_{\theta z}] \begin{Bmatrix} v_i \\ \theta_{zi} \\ v_j \\ \theta_{zj} \end{Bmatrix} \tag{22}$$

$$\{v(x)\} = [N_{v1} \quad N_{v2} \quad N_{v3} \quad N_{v4}] \begin{Bmatrix} v_i \\ \theta_{zi} \\ v_j \\ \theta_{zj} \end{Bmatrix} = [N_v] \begin{Bmatrix} v_i \\ \theta_{zi} \\ v_j \\ \theta_{zj} \end{Bmatrix} \tag{23}$$

$$\left\{\frac{dv}{dx}\right\} = [N'_{v1} \quad N'_{v2} \quad N'_{v3} \quad N'_{v4}] \begin{Bmatrix} v_i \\ \theta_{zi} \\ v_j \\ \theta_{zj} \end{Bmatrix} = [N'_v] \begin{Bmatrix} v_i \\ \theta_{zi} \\ v_j \\ \theta_{zj} \end{Bmatrix} \tag{24}$$

All shape functions and there first order derivatives are embedded in the appendix.
There are two ways to get the stiffness matrix: the first using the virtual displacements principal by solving the differential equations of the displacements (equations (11) to (16)), the second using the virtual forces principal by getting the flexibility matrix for one of the end nodes.

Deriving the element stiffness matrix from the flexibility matrix is easier, where getting the flexibility coefficients using the virtual forces principal depend on the equations of statics. The variations that may be occur in section or material properties do not affect the equations of statics.

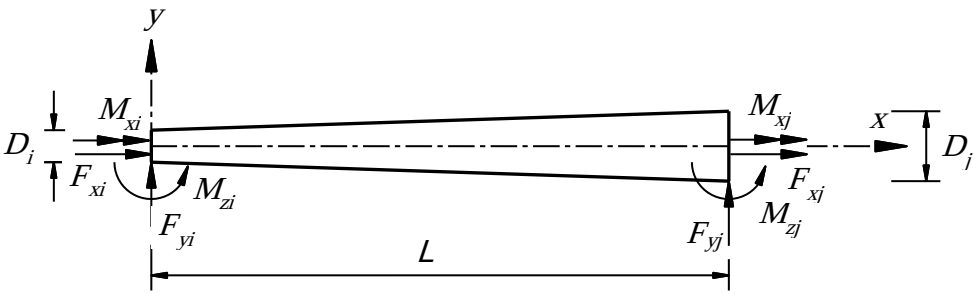

Figure 1: Tapered element in local *x-y* plan

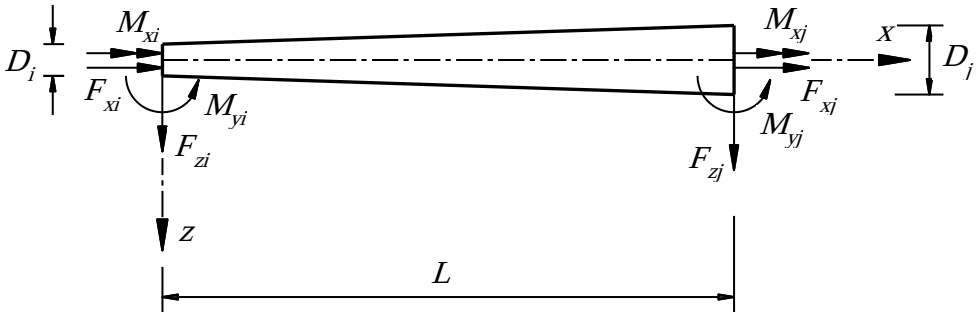

Figure 2: Tapered element in local x-z plan

From static equilibrium, the relationship between forces acting at nodes *i* and *j* are as shown:

$$\{F_i\}=[\varphi]\{F_j\} \tag{25}$$

$$\begin{Bmatrix} F_{xi} \\ F_{yi} \\ F_{zi} \\ M_{xi} \\ M_{yi} \\ M_{zi} \end{Bmatrix} = \begin{bmatrix} -1 & 0 & 0 & 0 & 0 & 0 \\ 0 & -1 & 0 & 0 & 0 & 0 \\ 0 & 0 & -1 & 0 & 0 & 0 \\ 0 & 0 & 0 & -1 & 0 & 0 \\ 0 & 0 & L & 0 & -1 & 0 \\ 0 & -L & 0 & 0 & 0 & -1 \end{bmatrix} \begin{Bmatrix} F_{xj} \\ F_{yj} \\ F_{zj} \\ M_{xj} \\ M_{yj} \\ M_{zj} \end{Bmatrix} \tag{26}$$

where [φ] is the static equilibrium matrix. The relationship between the internal real forces distributed along the element and joint *i* real forces are expressed as the following expressions:

$$\{F(x)\}=[Q]\{F_i\} \tag{27}$$

$$\begin{Bmatrix} F_x(x) \\ F_y(x) \\ F_z(x) \\ M_x(x) \\ M_y(x) \\ M_z(x) \end{Bmatrix} = \begin{bmatrix} 1 & 0 & 0 & 0 & 0 & 0 \\ 0 & 1 & 0 & 0 & 0 & 0 \\ 0 & 0 & 1 & 0 & 0 & 0 \\ 0 & 0 & 0 & 1 & 0 & 0 \\ 0 & 0 & -x & 0 & -1 & 0 \\ 0 & x & 0 & 0 & 0 & -1 \end{bmatrix} \begin{Bmatrix} F_{xi} \\ F_{yi} \\ F_{zi} \\ M_{xi} \\ M_{yi} \\ M_{zi} \end{Bmatrix} \tag{28}$$

where [*Q*] is the element force distribution matrix.

the flexibility coefficients for axial force, torsional moment and transverse shear force either in *y* or in *z* directions can be derived respectively as:

$$[d_A] = \int_0^L \{Q\}^T \frac{1}{EA(x)}[Q]dx = \frac{1}{E}\int_0^L \frac{dx}{A(x)} = \frac{L}{EA_i}\frac{1}{C_A} \tag{29}$$

$$[d_T] = \int_0^L \{Q\}^T \frac{1}{GJ(x)}[Q]dx = \frac{1}{G}\int_0^L \frac{dx}{J(x)} = \frac{L}{GJ_i}\frac{1}{C_J} \tag{30}$$

$$[d_S] = \int_0^L \{Q\}^T \frac{1}{G\kappa A(x)}[Q]dx = \frac{1}{G\kappa}\int_0^L \frac{dx}{A(x)} = \frac{L}{G\kappa A_i}\frac{1}{C_A} \tag{31}$$

while the flexibility coefficients for bending about *z* and *y* axes, respectively are given as:

$$[d_{Bz}] = \int_0^L \{Q\}^T \frac{1}{EI_z(x)}[Q]dx = \frac{1}{E}\int_0^L \begin{Bmatrix} x \\ -1 \end{Bmatrix} [x \quad -1] \frac{dx}{I_z(x)} \tag{32}$$

$$[d_{Bz}] = \frac{1}{E}\int_0^L \begin{bmatrix} x^2 & -x \\ -x & 1 \end{bmatrix} \frac{dx}{I_z(x)} = \frac{L}{EI_{zi}} \begin{bmatrix} \frac{p_z L^2}{3} & -C_{Fz}\frac{L}{2} \\ -C_{Fz}\frac{L}{2} & C_{Mz} \end{bmatrix} \tag{33}$$

$$[d_{By}] = \int_0^L \{Q\}^T \frac{1}{EI_y(x)} [Q] dx = \frac{1}{E} \int_0^L \begin{Bmatrix} -x \\ -1 \end{Bmatrix} [-x \quad -1] \frac{dx}{I_y(x)} \tag{34}$$

$$[d_{By}] = \frac{1}{E} \int_0^L \begin{bmatrix} x^2 & x \\ x & 1 \end{bmatrix} \frac{dx}{I_y(x)} = \frac{L}{EI_{yi}} \begin{bmatrix} \frac{p_y L^2}{3} & C_{Fy} \frac{L}{2} \\ C_{Fy} \frac{L}{2} & C_{My} \end{bmatrix} \tag{35}$$

By taking in consideration the effect of transverse shear on bending, the flexibility coefficients for combined shear and bending about *z* and *y* axes, respectively are given as:

$$[d_z] = [d_{Bz}] + [d_S] = \frac{L}{EI_{zi}} \begin{bmatrix} \frac{p_z L^2}{3} + \frac{\Phi_z L^2}{12} & -C_{Fz} \frac{L}{2} \\ -C_{Fz} \frac{L}{2} & C_{Mz} \end{bmatrix} \tag{36}$$

$$[d_y] = [d_{By}] + [d_S] = \frac{L}{EI_{yi}} \begin{bmatrix} \frac{p_y L^2}{3} + \frac{\Phi_y L^2}{12} & C_{Fy} \frac{L}{2} \\ C_{Fy} \frac{L}{2} & C_{My} \end{bmatrix} \tag{37}$$

Now, the flexibility matrix for node *i* can be presented as:

$$[d] = \begin{bmatrix} \frac{L}{EA_i} \frac{1}{C_A} & 0 & 0 & 0 & 0 & 0 \\ 0 & \frac{p_z L^3}{3EI_{zi}} + \frac{\Phi_z L^3}{12EI_{zi}} & 0 & 0 & 0 & -\frac{C_{Fz} L^2}{2EI_{zi}} \\ 0 & 0 & \frac{p_y L^3}{3EI_{yi}} + \frac{\Phi_y L^3}{12EI_{yi}} & 0 & \frac{C_{Fy} L^2}{2EI_{yi}} & 0 \\ 0 & 0 & 0 & \frac{L}{GJ_i} \frac{1}{C_J} & 0 & 0 \\ 0 & 0 & \frac{C_{Fy} L^2}{2EI_{yi}} & 0 & \frac{C_{My} L}{EI_{yi}} & 0 \\ 0 & -\frac{C_{Fz} L^2}{2EI_{zi}} & 0 & 0 & 0 & \frac{C_{Mz}}{EI_z} \end{bmatrix} \tag{38}$$

The exact element stiffness matrix in local coordinates can be calculated from the following formula:

$$[k'] = \begin{bmatrix} [d]^{-1} & [d]^{-1}[\varphi]^T \\ [\varphi][d]^{-1} & [\varphi][d]^{-1}[\varphi]^T \end{bmatrix} = \begin{bmatrix} [k'_A] & & & \\ & [k'_z] & & \\ & & [k'_T] & \\ & & & [k'_y] \end{bmatrix} \tag{39}$$

The submatrices can be calculated as:

$$[k'_A] = \frac{EA_i}{L} C_A \begin{bmatrix} 1 & -1 \\ -1 & 1 \end{bmatrix} \tag{40}$$

$$[k'_T] = \frac{GJ_i}{L} C_J \begin{bmatrix} 1 & -1 \\ -1 & 1 \end{bmatrix} \tag{41}$$

$$[k'_z] = \frac{EI_{zi}}{L^3 C_{Bz}} \begin{bmatrix} 12C_{Mz} & 6C_{Fz}L & -12C_{Mz} & (2C_{Mz}-C_{Fz})6L \\ 6C_{Fz}L & (4p_z+\Phi_z)L^2 & -6C_{Fz}L & \left(6C_{Fz}-(4p_z+\Phi_z)\right)L^2 \\ -12C_{Mz} & -6C_{Fz}L & 12C_{Mz} & -(2C_{Mz}-C_{Fz})6L \\ (2C_{Mz}-C_{Fz})6L & \left(6C_{Fz}-(4p_z+\Phi_z)\right)L^2 & -(2C_{Mz}-C_{Fz})6L & \left(12(C_{Mz}-C_{Fz})+(4p_z+\Phi_z)\right)L^2 \end{bmatrix} \tag{42}$$

$$[k'_y] = \frac{EI_{yi}}{L^3 C_{By}} \begin{bmatrix} 12C_{My} & -6C_{Fy}L & -12C_{My} & -(2C_{My}-C_{Fy})6L \\ -6C_{Fy}L & \left(4p_y+\Phi_y\right)L^2 & 6C_{Fy}L & \left(6C_{Fy}-\left(4p_y+\Phi_y\right)\right)L^2 \\ -12C_{My} & 6C_{Fy}L & 12C_{My} & (2C_{My}-C_{Fy})6L \\ -(2C_{My}-C_{Fy})6L & \left(6C_{Fy}-\left(4p_y+\Phi_y\right)\right)L^2 & (2C_{My}-C_{Fy})6L & \left(12(C_{My}-C_{Fy})+\left(4p_y+\Phi_y\right)\right)L^2 \end{bmatrix} \tag{43}$$

The stiffness coefficients are embedded in the appendix.
Finally, the element stiffness matrix in global coordinates can be calculated from the following expression:

$$[k]=[T]^{\mathrm{T}}[k'][T] \tag{44}$$

where:
[*k*]: is the 12x12 element stiffness matrix in global coordinates
[*k'*]: is the 12x12 element stiffness matrix in local coordinates
[*T*]: is the 12x12 transformation matrix which is explained in detail in different references as in *Logan* (2012) and *McGuire etc al*. (1999).

Element consistent mass matrix

The exact element consistent mass matrix for area and torsional moment of inertia can be performed using the following equations, respectively:

$$[m'_A] = \int_0^L \{N_A\}^T \rho [N_A] A(x) dx = \frac{\rho A_i C_A L}{6} \begin{bmatrix} 2 & 1 \\ 1 & 2 \end{bmatrix} \tag{45}$$

$$[m'_J] = \int_0^L \{N_J\}^T \rho [N_J] J(x) dx = \frac{\rho J_i C_J L}{6} \begin{bmatrix} 2 & 1 \\ 1 & 2 \end{bmatrix} \tag{46}$$

The exact consistent mass matrix for translational moment of inertia (about *z* or *y* axis) can be performed using the following equations:

$$[m'_f]=\int_0^L \{N_f\}^T \rho[N_f]A(x)dx = \begin{bmatrix} m'_{f11} & m'_{f12} & m'_{f13} & m'_{f14} \\ & m'_{f22} & m'_{f23} & m'_{f24} \\ & & m'_{f33} & m'_{f34} \\ & \text{Symm.} & & m'_{f44} \end{bmatrix} \quad (47)$$

the general equation that presents the elements of the consistent mass matrix for translational moment of inertia is calculated as:

$$m'_{fkl}=\rho \int_0^L N_{fk}(x)\, N_{fl}(x)A(x)dx \quad (48)$$

$$m'_{fkl}=\frac{\rho A_i L}{C_{Bs}^2}[I_{f1}+I_{f2}+I_{f3}+I_{f4}],\ k \text{ and } l=1,\ 2,\ 3,\ 4 \quad (49)$$

while the exact consistent mass matrix for rotatory moment of inertia about *z* or *y* axes can be performed using the following equation:

$$[m'_{\theta s}]=\int_0^L \{N_{\theta s}\}^T \rho[N_{\theta s}]I_s(x)dx = \begin{bmatrix} m'_{\theta s11} & m'_{\theta s12} & m_{\theta s13} & m'_{\theta s14} \\ & m'_{\theta s22} & m'_{\theta s23} & m'_{\theta s24} \\ & & m'_{\theta s33} & m'_{\theta s34} \\ & \text{Symm.} & & m'_{\theta s44} \end{bmatrix} \quad (50)$$

where *s* denotes the axis *z* or *y*

the general equation that presents the elements of the consistent mass matrix for rotatory moment of inertia is calculated as:

$$m'_{\theta skl}=\rho \int_0^L N_{\theta sk}(x)\, N_{\theta sl}(x)I_s(x)dx \quad (51)$$

$$m'_{\theta skl}=\frac{\rho A_i L}{C_{Bs}^2}\left(\frac{r_{Gi}}{L}\right)^2[I_{\theta s1}+I_{\theta s2}],\ k \text{ and } l=1,2,3,4 \quad (52)$$

where:
r_{Gi} is the radius of gyration at the start node *i* and can be performed as:

$$r_{Gi}=\sqrt{\frac{I_{si}}{A_i}} \quad (53)$$

The element full consistent mass matrix in local coordinates can be performed using the following equation:

$$[m']=\begin{bmatrix}[m'_A] & & & \\ & [m'_{\theta z}]+[m'_v] & & \\ & & [m'_J] & \\ & & & [m'_{\theta y}]+[m'_w]\end{bmatrix} \tag{54}$$

To include the effect of transverse shear on bending, the bending (about *z* or *y* axes) consistent mass matrix equals the sum of consistent rotatory and translational mass matrices.

Element geometric stiffness matrix

For nonlinear analysis, it is necessary to find the geometric stiffness matrix that represents the change in stiffness due to second order effects of the deformations. The effect of combined axial-bending and axial-torsion is considered in the present study. The effect of combined torsion-bending is not considered, where this effect is negligible in symmetric or bisymmetric sections. It should be noted that this study also did not touch on with nonuniform torsion.
According to *McGuire etc al*. (1999), the nonlinear terms of the finite internal virtual work done can be performed using the following equation:

$$\delta W_{int}=\frac{1}{2}\int_L F_{xi}\delta\left[\left(\frac{\partial u}{\partial x}\right)^2+\left(\frac{\partial v}{\partial x}\right)^2+\left(\frac{\partial w}{\partial x}\right)^2\right]dx+\frac{1}{2}\int_L \frac{F_{xi}J(x)}{A(x)}\delta\left(\frac{\partial \theta_x}{\partial x}\right)^2 dx \tag{55}$$

The element geometric stiffness matrix in local coordinates can be performed using the following equation:

$$[k'_g]=F_{xi}\int_0^L\left[\{N'_u\}^T[N'_u]+\{N'_v\}^T[N'_v]+\{N'_w\}^T[N'_w]\right]dx+F_{xi}\int_0^L\frac{J(x)}{A(x)}\{N'_{\theta x}\}^T[N'_{\theta x}]dx \tag{56}$$

where $[N_u]$, $[N_v]$, $[N_w]$ and $[N_{\theta x}]$ are the shape functions for the respective displacement coordinates.

writing the element geometric stiffness matrix with combining the submatrices as:

$$[k'_g]=\begin{bmatrix}[k'_{gA}] & & & \\ & [k'_{gz}] & & \\ & & [k'_{gJ}] & \\ & & & [k'_{gy}]\end{bmatrix} \tag{57}$$

The element geometric stiffness matrices for axial force and torsion can be performed using the following equations:

$$[k'_{gA}]=\frac{F_{xi}}{L}C_{gA}\begin{bmatrix}1 & -1\\ -1 & 1\end{bmatrix} \tag{58}$$

$$[k'_{gT}]=\frac{F_{xi}I_{pi}}{A_iL}C_{gT}\begin{bmatrix}1 & -1\\ -1 & 1\end{bmatrix} \tag{59}$$

while, the element geometric stiffness matrix for combined axial force and bending (about *z* or *y* axes) in local coordinates can be performed using the following equation:

$$[k'_{gs}]=\begin{bmatrix} k'_{gs11} & k'_{gs12} & k'_{gs13} & k'_{gs14} \\ & k'_{gs22} & k'_{gs23} & k'_{gs24} \\ & & k'_{gs33} & k'_{gs34} \\ & \text{Symm.} & & k'_{gs44} \end{bmatrix} \tag{60}$$

where *s* denotes the axis *z* or *y*.
the general equation that presents the elements of the previous matrix is:

$$k'_{gfkl}=F_{xi}\int_0^L N'_{fk}(x)\,N'_{fl}(x)dx \tag{61}$$

$$k'_{gfkl}=\frac{F_{xi}}{C_{Bs}^2 L}\left[I_{gf1}+I_{gf2}+I_{gf3}+I_{gf4}\right],\ k \text{ and } l=1,\ 2,\ 3,\ 4 \tag{62}$$

The geometric stiffness coefficients are found in the appendix.

VERIFICATION OF THE PRESENT MODEL

Linear stability analysis of tapered cantilevers

This verification examines the efficiency of the element both linear and geometric stiffness matrices. *Bai etc. al.* (2018) studied the elastic buckling load for eight section types. In this verification, the four sections shown in Figure 3: were chosen to get the elastic critical load using the proposed FE model.
All members are cantilever with fixed support at the larger end and subjected to compressive force at the free smaller end. All members are 20 m long, and the section dimensions are given below figures.
The materials of hollow and solid sections are assumed as steel. The *Young's* modulus, *Poisson's* ratio and density of steel are 205 Gpa, 0.3 and 7.7×10^3 kg/ m^3, respectively. The results of the elastic buckling load calculated using the proposed FE were compared with the results of *Bai etc. al.* (2018) as seen from Figure 4: to Figure 11:. The comparison illustrates that using 2 elements from the proposed FE model gave results as those of more than 50 stepped elements with error less than 1%. It is obvious from the shown figures that convergence occurs using the proposed model faster than the model of *Bai etc. al.* (2018).

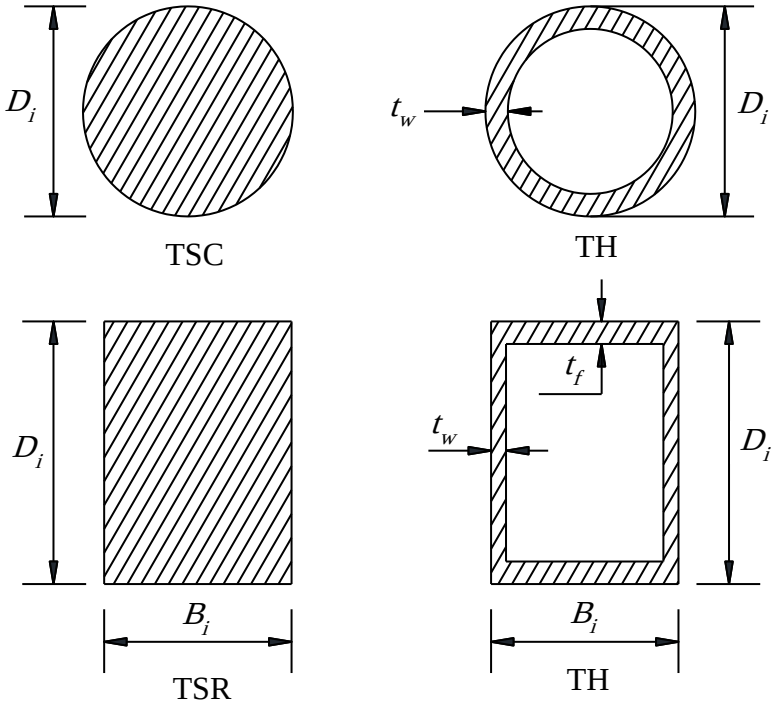

Figure 3: Tapered sections at thin end *i* used in verifications 1 and 2

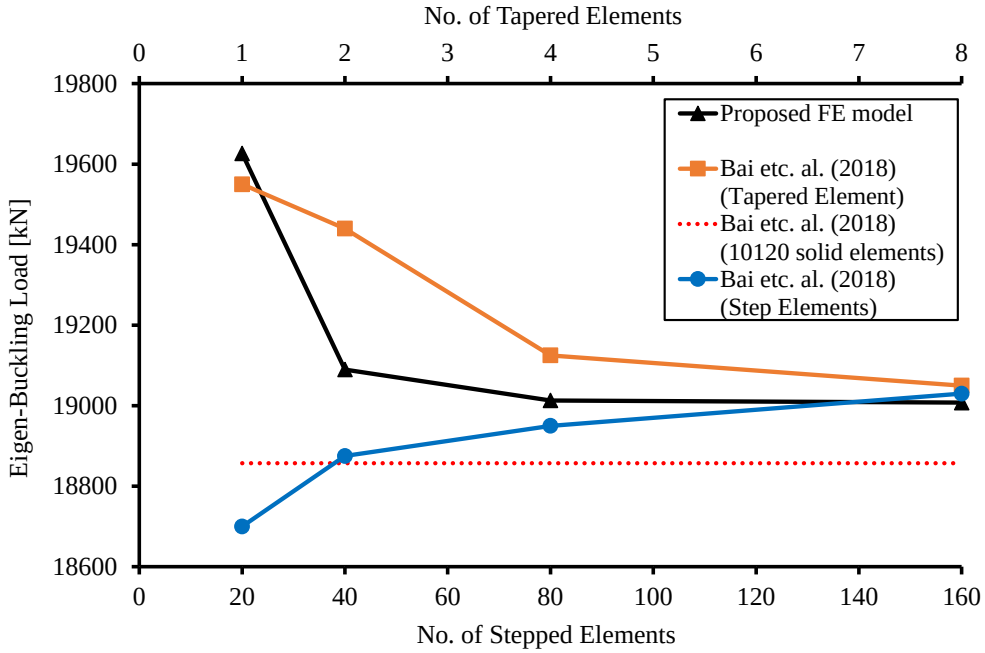

Figure 4: Elastic critical load for TSC (D_1 = 0.4 m, D_2 = 1 m)

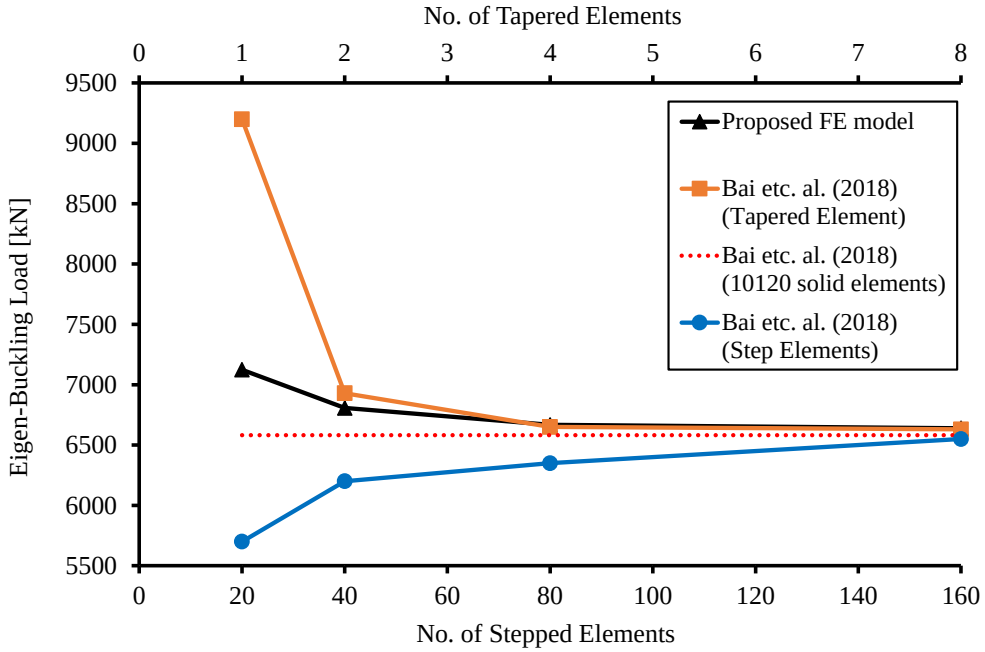

Figure 5: Elastic critical load for TSC (D_1 = 0.2 m, D_2 = 1 m)

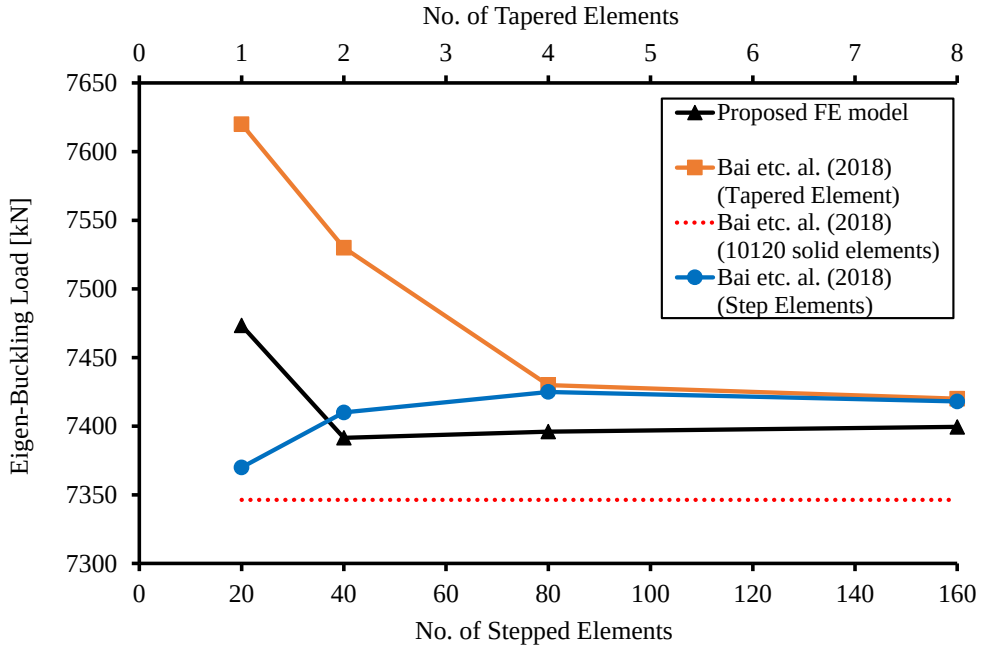

Figure 6: Elastic critical load for THC (D_1 = 0.4 m, D_2 = 1 m, t = 0.04 m)

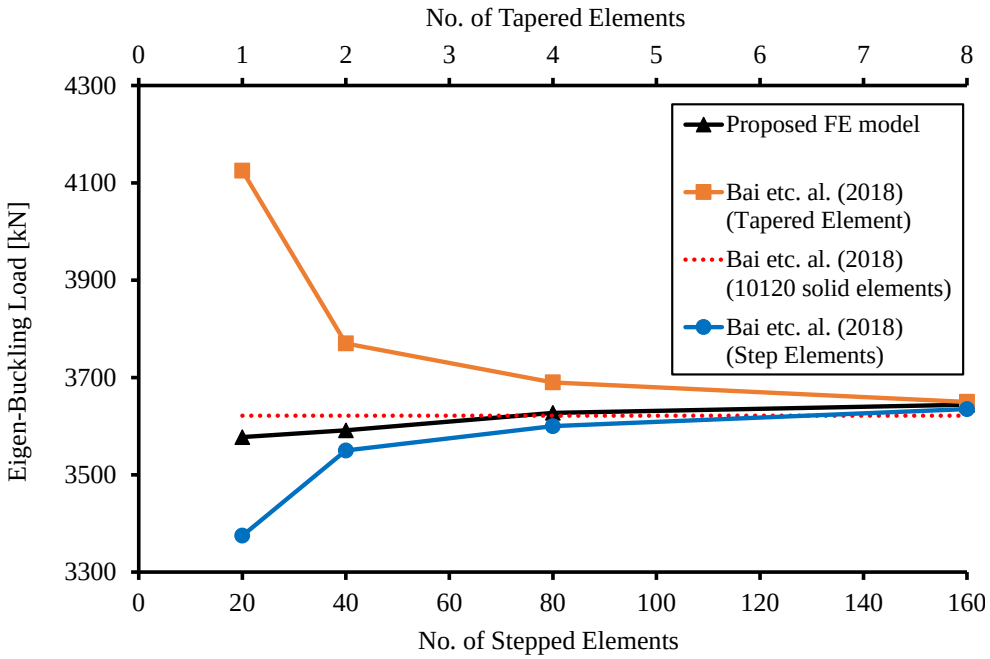

Figure 7: Elastic critical load for THC (D_1 = 0.2 m, D_2 = 1 m, t = 0.04 m)

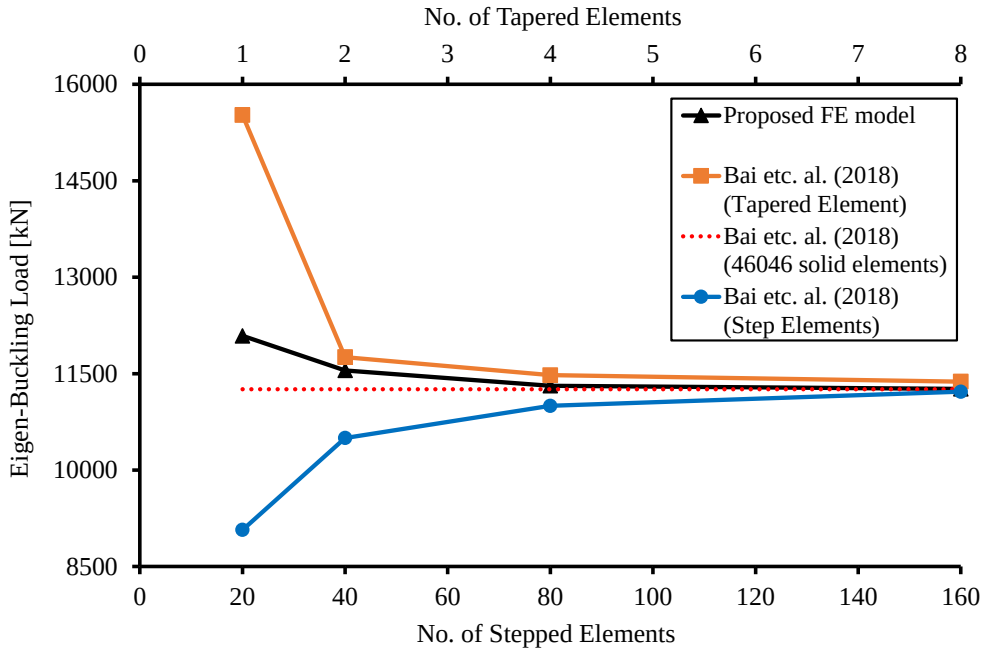

Figure 8: Elastic critical load for TSR (D_1 = B_1= 0.2 m, D_2 = B_2 = 1 m)

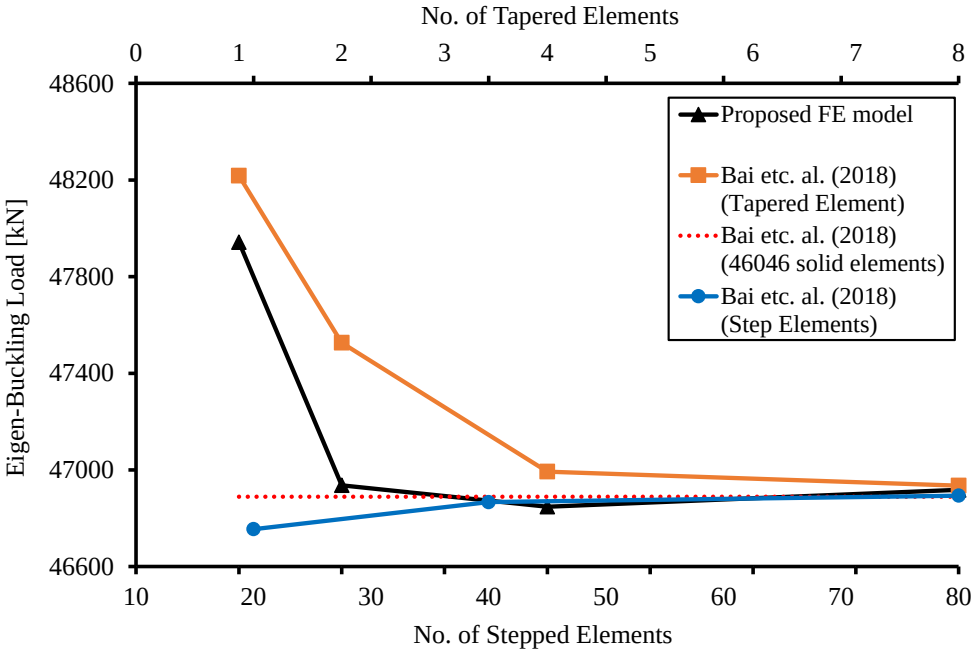

Figure 9: Elastic critical load for TSR (D_1 = 0.4 m, D_2 = 1 m, B_1= B_2=1 m)

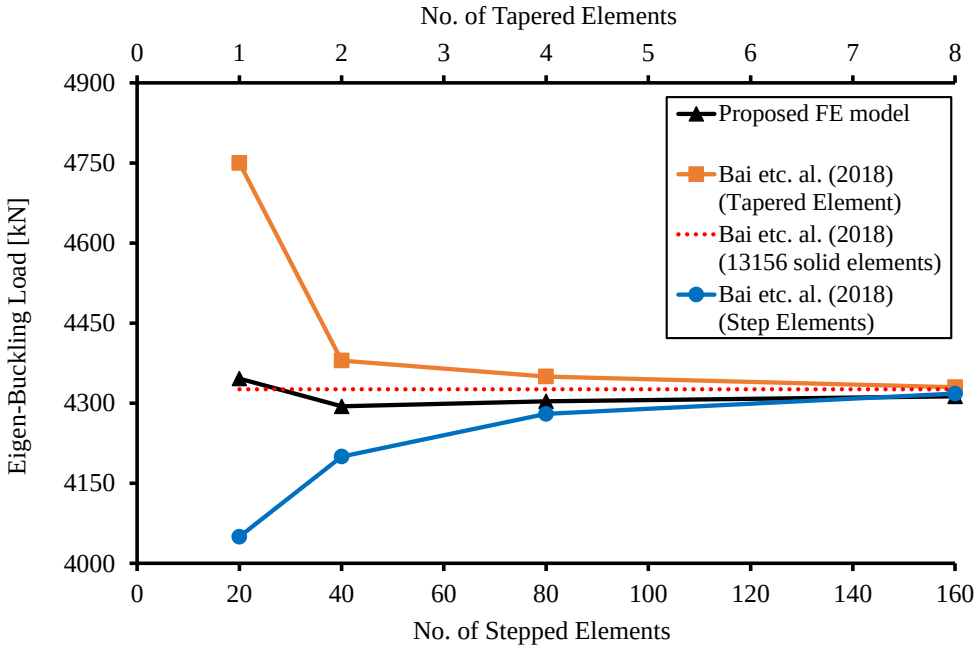

Figure 10: Elastic critical load for THR (D_1 = B_1= 0.2 m, D_2 = B_2 = 1 m, t_f = 0.04 m, t_w = 0.02 m)

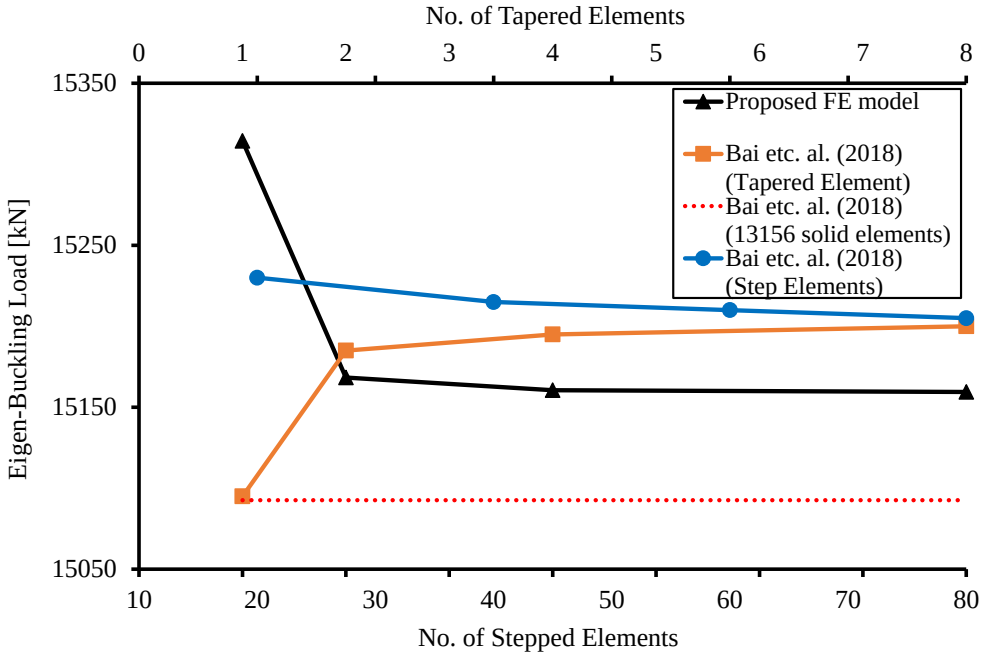

Figure 11: Elastic critical load for THR (D_1 = 0.4 m, D_2 = 1 m, B_1= B_2=1 m, t_f = 0.04 m, t_w = 0.02 m)

Modal analysis of tapered cantilevers

Bai etc. al. (2018) presented modal analysis for cantilevers with different tapered sections. The four tapered sections shown in Figure 3: are chosen to verify the proposed FE model. All members are 10 m long, and the section dimensions are given as:

- The solid circular section's diameter changes from 800 to 200 mm.
- The hollow circular section's diameter changes from 400 to 100 mm with thickness 20 mm.
- The solid rectangular section's depth and breadth change from 1000 to 250 and 800 to 200 mm, respectively.
- The hollow rectangular section's depth and breadth change from 800 to 200 and 400 to 100 mm, respectively. Flange and web thicknesses are 25 and 10 mm, respectively.

The materials of hollow and solid sections are assumed as steel and concrete, respectively. The *Young's* modulus, *Poisson's* ratio and density of steel are 205 Gpa, 0.3 and 7.7×10^3 kg/ m^3, respectively; the corresponding values of concrete are 30 Gpa, 0.2 and 2.4×10^3 kg/ m^3. The results of the proposed FE are compared with those of *Bai etc. al.* (2018) and with results of the commercial software ARSAP as shown in Table 1:, 0, 0Table 3: and Table 4:. The comparison illustrates the efficiency and accuracy of the proposed model.

Table 1: Natural frequencies [Hz] for tapered solid circular section (TSC).

Mode	Mode type	Number of proposed FE [-]			6623 solid elements	*Bai etc. al.* (2018)		
		2	4	8		6048 solid elements	2 FE	4 FE
1	Flexural	6.59	6.54	6.53	6.52	6.52	6.56	6.55
2	Flexural	20.87	20.69	20.60	20.60			
3	Flexural		46.03	45.60	45.78			
4	Flexural		83.94	81.75	82.37			
5	Torsional			122.53	123.81			
7	Axial	131.00	137.17	137.96	132.92			

Table 2: Natural frequencies [Hz] for tapered hollow circular section (THC).

Mode	Mode type	Number of proposed FE [-]			32100 Solid elements	*Bai etc. al.* (2018)		
		2	4	8		2016 solid elements	2 FE	4 FE
1	Flexural	4.74	4.71	4.70	4.70	4.72	4.81	4.74
2	Flexural	17.66	17.49	17.26	17.41			
3	Flexural		41.13	40.45	40.77			
4	Flexural		77.40	73.74	74.76			
6	Torsional	139.66	152.54	154.63	154.84			
7	Axial	165.07	167.88	168.05	167.51			

Table 3: Natural frequencies [Hz] for tapered solid rectangular section (TSR).

Mode	Mode type	Number of proposed FE [-]			22491 solid elements	*Bai etc. al.* (2018)		
		2	4	8		6300 solid elements	2 FE	4 FE
1	Flexural	7.60	7.54	7.53	7.55	7.54	7.32	7.49
2	Flexural	9.49	9.40	9.39	9.31			
3	Flexural	24.02	23.78	23.69	24.08			
4	Flexural	29.83	29.50	29.35	29.38			
5	Flexural		52.70	52.26	53.57			
6	Flexural		64.80	64.17	64.71			
8	Torsional			109.69	110.01			
10	Axial			138.45	131.713			

Table 4: Natural frequencies [Hz] for tapered hollow rectangular section (THR).

Mode	Mode type	Number of proposed FE [-]			5100 Shell elements	*Bai etc. al.* (2018)		
		2	4	8		4284 solid elements	2 FE	4 FE
1	Flexural	5.39	5.36	5.35	5.37	5.37	5.47	5.39
2	Flexural	11.22	11.15	11.14	11.12			
3	Flexural	20.23	20.17	20.11	20.08			
4	Flexural	41.34	41.04	40.85	40.64			
5	Flexural		47.50	47.17	46.58			
22	Axial	163.75	166.13	166.27	164.67			

Modal analysis of NREL 5 MW reference wind turbine with fixed base

In this verification, *Yung-Yen Ko* (2020) used the NREL (National Renewable Energy Laboratory) 5 MW reference wind turbine to verify his model. *Yung-Yen Ko* (2020) presented a closed-form solution to calculate the first natural frequency of offshore wind turbines. The model simulates the towers as SDOF tapered structures with rigid or flexible base based on *Rayleigh's* theory. *Yung-Yen Ko* (2020) compared the results of his model with the results of the chosen wind turbine that were performed by *Jonkman etc. al.* (2009) using the advanced wind turbine analysis programs FAST and ADAMS.
The data of wind turbine geometry and material are shown in Table 5:. The wind turbine is modelled using the proposed FE approach to verify the accuracy of the model used in the present study. Dividing the tower into two finite elements gave results with heigh accuracy. The results of the present study were compared with those of *Yung-Yen Ko* (2020), FAST and ADAMS codes. It's obvious that the model of *Yung-Yen Ko* (2020) estimates only the first natural of frequency, because this mode is a SDOF model. The second natural frequency result in the present study were compared with those of FAST and ADAMS codes and it was in the range of results. Table 6: shows the comparison between the present study (considering *Euler-Bernoulli* and *Timoshenko* models) and the results cited by *Yung-Yen Ko* (2020).

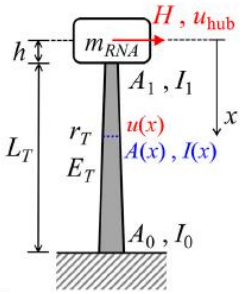

Figure 12: Structural model for a tapered wind turbine tower with fixed base

Table 5: NREL 5 MW reference wind turbine data

Material				
Young's modulus	E	=	2.10×10^8	[kN/ m^2]
Poisson's ratio	ν	=	0.3	[-]
Mass density	γ	=	8.5	[t/ m^3]
Geometry				
Top diameter	D_t	=	3.87	[m]
Bottom diameter	D_b	=	6.0	[m]
Tower height	H	=	87.6	[m]
Tower top thickness	t_t	=	0.0247	[m]
Tower bottom thickness	t_b	=	0.0351	[m]

Table 6: The first two natural frequencies [Hz] of NREL 5 MW reference wind turbine with fixed base

Mode	1st tower fore-aft	1st tower side-to-side	2nd tower fore-aft	2nd tower side-to-side
FAST	0.3240	0.3120	2.9003	2.9361
ADAMS	0.3195	0.3164	2.8590	2.9408
Present study (*E-B*)	0.3187		2.9130	
Present study (*T*)	0.3172		2.8038	
Yung-Yen Ko (2020)	0.2807~0.3248		-	

Application using the presented model

In this section, a static and modal analysis were carried out using the proposed FE model to show the efficiency of the model compared with other available commercial models. The data of the tower were chosen from the reference *Hu etc al.* (2014). *Hu etc al.* (2014) used three towers with different three heights in the analysis. In this paper, one of the towers is chosen to apply the proposed model on it. The tower material, geometry and applied static loads data are shown in Table 7: and Figure 13:.

Table 7: Tower material and geometry data used in static and modal analysis

Material				
Young's modulus	E	=	2.05×10^8	[kN/ m^2]
Poisson's ratio	ν	=	0.3	[-]
Mass density	γ	=	7.85	[t/ m^3]
Geometry				
Top diameter	D_t	=	5.7	[m]
Bottom diameter	D_b	=	8.5	[m]
Tower height	H	=	150	[m]
Tower thickness	t	=	0.3	[m]

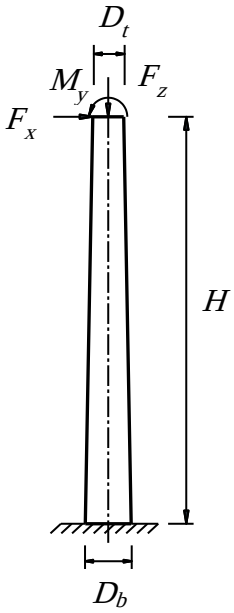

Figure 13: The tower dimensions with applied static loads

Consider the tower is subjected to the static loads: horizontal force of 850 [kN], vertical force of 750 [kN] downwards and anticlockwise bending moment of 400 [kN.m]. Analyzing the tower with the subjected loads needs only a single element of the proposed FE model. The results were compared with those of the commercial program MIDAS GEN. the tower was modeled with 5 and 10 beam elements, respectively. The comparison shown in Table 8: illustrates that a single element of the proposed FE model gives the same results of 10 beam elements in MIDAS GEN program in static analysis. This proves the efficiency of the model in static analysis.

Table 8: Displacements of the tower tip

Displacement	Proposed FE (1 element)	MIDAS GEN (5 elements)	MIDAS GEN (10 elements)
Horizontal [mm]	97.047	96.806	97.018
Vertical [mm]	8.687×10^{-2}	8.687×10^{-2}	8.687×10^{-2}
Rotation [rad.]	1.07972×10^{-3}	1.07636×10^{-3}	1.07898×10^{-3}

Modal analysis was made using the proposed FE model, and the results were compared with those of the commercial program ARSAP. The tower was modelled using 20, 100 and beam elements in ARSAP program. The natural frequencies were compared and tabulated in Table 9:.

Table 9: Natural frequencies [Hz] of the tower

Mode	Mode type	Number of proposed FE [-]		Number of ARSAP elements [-]		
		2	4	20	100	200
1	Flexural	0.386	0.386	0.399	0.398	0.396
2	Flexural	2.024	2.007	2.118	2.083	2.050
3	Flexural		5.244	5.619	5.411	5.224
4	Flexural		9.8789	10.775	10.081	9.507
6	Torsional	6.555	6.659	6.629	6.629	6.629
7	Axial	9.347	9.276	9.219	9.217	9.217

CONCLUSIONS

The present paper proposes a finite element formulation for Timoshenko non-prismatic beam-column elements based on exact shape functions of displacements. Both stiffness and consistent mass matrices are derived and given in detail. Verification examples has been made to validate the accuracy and efficiency of the proposed model in elastic stability and modal analysis. The proposed model gave very good responses in the analysis for different section types. The proposed model is applied to make static and modal analysis of a wind turbine tower. The static and modal results were compared with those of commercial programs MIDAS GEN and ARSAP, respectively. In static analysis, only single proposed element is enough to calculate the tip displacements and give results as exact results. In modal analysis, the natural frequencies have been obtained by ignoring the mass of nacelle-rotor system at the top of the tower. However, such concentrated mass should be considered because it can account for more than 30% of the total tower mass. Only two proposed elements are enough to calculate the first two flexural modes and the first torsional mode and axial mode. Doubling the number of elements lead to get two other flexural modes with high accuracy. The main significance in this study, when comparing with available models, is the great reduction in computational efforts by its numerical efficiency. The present study is considered to be essential for analyzing non-prismatic elements in modern structures, especially in analyzing wind turbine towers.

APPENDIX

Shape functions and there first derivatives

$$\xi_A = \begin{cases} \lim\limits_{r_A \to 0} \xi_A = \dfrac{x}{L} & \Gamma=0 \\ \dfrac{\ln\left(1+r_A \dfrac{x}{L}\right)}{\ln(1+r_A)} & \Gamma=1 \\ \left(\dfrac{1+r_A}{1+r_A \dfrac{x}{L}}\right)\dfrac{x}{L} & \Gamma=2 \end{cases} \tag{63}$$

$$\xi'_A = \begin{cases} \lim\limits_{r_h \to 0} \xi'_A = \dfrac{1}{L} & \Gamma=0 \\ \dfrac{C_A}{L}\dfrac{1}{\left(1+r_A \dfrac{x}{L}\right)} & \Gamma=1 \\ \dfrac{C_A}{L}\dfrac{1}{\left(1+r_A \dfrac{x}{L}\right)^2} & \Gamma=2 \end{cases} \tag{64}$$

$$\xi_J = \frac{1-\left(1+r_A \dfrac{x}{L}\right)^{(1-\Gamma_J)}}{1-(1+r_A)^{(1-\Gamma_J)}} \tag{65}$$

$$\xi'_J = \frac{C_J}{L}\frac{1}{\left(1+r_A\frac{x}{L}\right)^{\bar{\Gamma}_J}} \tag{66}$$

The exact shape functions for flexural displacements and rotations with their first derivatives are presented using the following equations:

$$N_{\theta sl} = \frac{1}{C_{Bs}}\left[A_{sl}\frac{\xi_h^{-(\bar{\Gamma}-2)}}{(\bar{\Gamma}-2)} + B_{sl}\frac{\xi_h^{-(\bar{\Gamma}-1)}}{(\bar{\Gamma}-1)} + C_{sl}\frac{1}{(\bar{\Gamma}-2)(\bar{\Gamma}-1)}\right] \tag{67}$$

$$N'_{\theta sl} = \frac{1}{C_{Bs}}\left(\frac{r_A}{L}\right)\left[-A_{sl}\xi_h^{-(\bar{\Gamma}-1)} - B_{sl}\xi_h^{-\bar{\Gamma}}\right] \tag{68}$$

$$N_{fl} = \frac{1}{C_{Bs}}\left(\frac{L}{r_A}\right)\left[-A_{sl}\frac{\xi_h^{-(\bar{\Gamma}-3)}}{(\bar{\Gamma}-2)(\bar{\Gamma}-3)} - B_{sl}\frac{\xi_h^{-(\bar{\Gamma}-2)}}{(\bar{\Gamma}-2)(\bar{\Gamma}-1)} + C_{sl}\frac{\xi_h}{(\bar{\Gamma}-2)(\bar{\Gamma}-1)} + D_{sl}\frac{\xi_h^{-(\Gamma-1)}}{(\Gamma-1)} + E_{sl}\right] \tag{69}$$

$$N'_{fl} = \frac{1}{C_{Bs}}\left[A_{sl}\frac{\xi_h^{-(\bar{\Gamma}-2)}}{(\bar{\Gamma}-2)} + B_{sl}\frac{\xi_h^{-(\bar{\Gamma}-1)}}{(\bar{\Gamma}-1)} + C_{sl}\frac{1}{(\bar{\Gamma}-2)(\bar{\Gamma}-1)} - D_{sl}\,\xi_h^{-\Gamma}\right] \tag{70}$$

where the subscripts:
$\ell = 1, 2, 3, 4$
$s = z$ or y axis
$f = v$ or w
and

$$\xi_h = \left(1+r_A\frac{x}{L}\right),\ dx = \frac{L}{r_A}d\xi_h \tag{71}$$

Table 10: Coefficients of flexure shape functions Azℓ, Bzℓ and Czℓ for bending about z

ℓ	$A_{z\ell}$	$B_{z\ell}$	$C_{z\ell}$
1	$-\frac{12C_{Mz}}{L^3}\left(\frac{L}{r_A}\right)^2$	$\frac{12C_{Mz}}{L^3}\left(\frac{L}{r_A}\right)^2 + \frac{6C_{Fz}}{L^2}\left(\frac{L}{r_A}\right)$	$-\left(A_{z1}(\bar{\Gamma}-1)+B_{z1}(\bar{\Gamma}-2)\right)$
2	$-\frac{6C_{Fz}}{L^2}\left(\frac{L}{r_A}\right)^2$	$\frac{6C_{Fz}}{L^2}\left(\frac{L}{r_A}\right)^2 + \frac{(4p_z+\Phi_z)}{L}\left(\frac{L}{r_A}\right)$	$-\left(A_{z2}(\bar{\Gamma}-1)+B_{z2}(\bar{\Gamma}-2)\right.$ $\left.+C_{Bz}(\bar{\Gamma}-2)(\bar{\Gamma}-1)\right)$
3	$\frac{12C_{Mz}}{L^3}\left(\frac{L}{r_A}\right)^2$	$-\frac{12C_{Mz}}{L^3}\left(\frac{L}{r_A}\right)^2 - \frac{6C_{Fz}}{L^2}\left(\frac{L}{r_A}\right)$	$-\left(A_{z3}(\bar{\Gamma}-1)+B_{z3}(\bar{\Gamma}-2)\right)$
4	$-\frac{(12C_{Mz}-6C_{Fz})}{L^2}\left(\frac{L}{r_A}\right.$	$\frac{(12C_{Mz}-6C_{Fz})}{L^2}\left(\frac{L}{r_A}\right)^2 + \frac{\left(6C_{Fz}-(4p_z+\Phi_z\right.}{L}$	$-\left(A_{z4}(\bar{\Gamma}-1)+B_{z4}(\bar{\Gamma}-2)\right)$

Table 11: Coefficients of flexure shape functions Dzℓ and Ezℓ

ℓ	$D_{z\ell}$	$E_{z\ell}$
1	$\frac{12C_{Mz}}{L^3}\left(\frac{C_A}{r_A}\frac{\Phi_z L^3}{12}\right)\left(\frac{r_A}{L}\right)$	$\frac{A_{zl}}{(\bar{\Gamma}\text{-}2)(\bar{\Gamma}\text{-}3)}-\frac{D_{zl}}{(\Gamma\text{-}1)}+\frac{6C_{Fz}}{L^2}\left(\frac{L}{r_A}\right)\frac{1}{(\bar{\Gamma}\text{-}2)}+C_{Bz}\left(\frac{r_A}{L}\right)$
2	$\frac{6C_{Fz}}{L^2}\left(\frac{C_A}{r_A}\frac{\Phi_z L^3}{12}\right)\left(\frac{r_A}{L}\right)$	$\frac{A_{zl}}{(\bar{\Gamma}\text{-}2)(\bar{\Gamma}\text{-}3)}-\frac{D_{zl}}{(\Gamma\text{-}1)}+\frac{(4p_z+\Phi_z)}{L}\left(\frac{L}{r_A}\right)\frac{1}{(\bar{\Gamma}\text{-}2)}-C_{Bz}$
3	$-\frac{12C_{Mz}}{L^3}\left(\frac{C_A}{r_A}\frac{\Phi_z L^3}{12}\right)\left(\frac{r_A}{L}\right)$	$\frac{A_{zl}}{(\bar{\Gamma}\text{-}2)(\bar{\Gamma}\text{-}3)}-\frac{D_{zl}}{(\Gamma\text{-}1)}-\frac{6C_{Fz}}{L^2}\left(\frac{L}{r_A}\right)\frac{1}{(\bar{\Gamma}\text{-}2)}$
4	$\frac{(12C_{Mz}\text{-}6C_{Fz})}{L^2}\left(\frac{C_A}{r_A}\frac{\Phi_z L^3}{12}\right)\left(\frac{r_A}{L}\right.$	$\frac{A_{zl}}{(\bar{\Gamma}\text{-}2)(\bar{\Gamma}\text{-}3)}-\frac{D_{zl}}{(\Gamma\text{-}1)}+\frac{\left(6C_{Fz}\text{-}(4p_z+\Phi_z)\right)}{L}\left(\frac{L}{r_A}\right)\frac{1}{(\bar{\Gamma}\text{-}2)}$

Table 12: Coefficients of flexure shape functions Ayℓ, Byℓ and Cyℓ for bending about y

ℓ	$A_{y\ell}$	$B_{y\ell}$	$C_{y\ell}$
1	$-\frac{12C_{My}}{L^3}\left(\frac{L}{r_A}\right)^2$	$\frac{12C_{My}}{L^3}\left(\frac{L}{r_A}\right)^2+\frac{6C_{Fy}}{L^2}\left(\frac{L}{r_A}\right)$	$-\left(A_{y1}(\bar{\Gamma}\text{-}1)+B_{y1}(\bar{\Gamma}\text{-}2)\right.$
2	$\frac{6C_{Fy}}{L^2}\left(\frac{L}{r_A}\right)^2$	$-\frac{6C_{Fy}}{L^2}\left(\frac{L}{r_A}\right)^2-\frac{\left(4p_y+\Phi_y\right)}{L}\left(\frac{L}{r_A}\right)$	$-\left(A_{y2}(\bar{\Gamma}\text{-}1)+B_{y2}(\bar{\Gamma}\text{-}2)\right.$ $-C_{By}(\bar{\Gamma}\text{-}2)(\bar{\Gamma}\text{-}1)$
3	$\frac{12C_{My}}{L^3}\left(\frac{L}{r_A}\right)^2$	$-\frac{12C_{My}}{L^3}\left(\frac{L}{r_A}\right)^2-\frac{6C_{Fy}}{L^2}\left(\frac{L}{r_A}\right)$	$-\left(A_{y3}(\bar{\Gamma}\text{-}1)+B_{y3}(\bar{\Gamma}\text{-}2)\right.$
4	$\frac{(12C_{My}\text{-}6C_{Fy})}{L^2}\left(\frac{L}{r_A}\right)^2$	$-\frac{(12C_{My}\text{-}6C_{Fy})}{L^2}\left(\frac{L}{r_A}\right)^2-\frac{\left(6C_{Fy}\text{-}\left(4p_y+\Phi_y\right)\right.}{L}$	$-\left(A_{y4}(\bar{\Gamma}\text{-}1)+B_{y4}(\bar{\Gamma}\text{-}2)\right.$

Table 13: Coefficients of flexure shape functions Dyℓ and Eyℓ

ℓ	$D_{y\ell}$	$E_{y\ell}$
1	$\frac{12C_{My}}{L^3}\left(\frac{C_A}{r_A}\frac{\Phi_y L^3}{12}\right)\left(\frac{r_A}{L}\right)$	$\frac{A_{yl}}{(\bar{\Gamma}-2)(\bar{\Gamma}-3)}-\frac{D_{yl}}{(\Gamma-1)}+\frac{6C_{Fy}}{L^2}\left(\frac{L}{r_A}\right)\frac{1}{(\bar{\Gamma}-2)}+C_{By}\left(\frac{r_A}{L}\right)$
2	$-\frac{6C_{Fy}}{L^2}\left(\frac{C_A}{r_A}\frac{\Phi_y L^3}{12}\right)\left(\frac{r_A}{L}\right)$	$\frac{A_{yl}}{(\bar{\Gamma}-2)(\bar{\Gamma}-3)}-\frac{D_{yl}}{(\Gamma-1)}-\frac{\left(4p_y+\Phi_y\right)}{L}\left(\frac{L}{r_A}\right)\frac{1}{(\bar{\Gamma}-2)}+C_{By}$
3	$-\frac{12C_{My}}{L^3}\left(\frac{C_A}{r_A}\frac{\Phi_y L^3}{12}\right)\left(\frac{r_A}{L}\right)$	$\frac{A_{yl}}{(\bar{\Gamma}-2)(\bar{\Gamma}-3)}-\frac{D_{yl}}{(\Gamma-1)}-\frac{6C_{Fy}}{L^2}\left(\frac{L}{r_A}\right)\frac{1}{(\bar{\Gamma}-2)}$
4	$-\frac{(12C_{My}-6C_{Fy})}{L^2}\left(\frac{C_A}{r_A}\frac{\Phi_y L^3}{12}\right)\left(\frac{r_A}{L}\right.$	$\frac{A_{yl}}{(\bar{\Gamma}-2)(\bar{\Gamma}-3)}-\frac{D_{yl}}{(\Gamma-1)}-\frac{\left(6C_{Fy}-\left(4p_y+\Phi_y\right)\right)}{L}\left(\frac{L}{r_A}\right)\frac{1}{(\bar{\Gamma}-2)}$

It should be noted that:

- The shape functions corresponding to the right and left rotations about *z* axis (θ_{zi}, θ_{zj}) differs in sign from the shape functions corresponding to the left and right rotations about *y* axis (θ_{yi}, θ_{yj}).
- The shape functions corresponding to displacements (v_{zi}, v_{zj}) and (w_{zi}, w_{zj}) have the same sign.

For square, circular, hollow square and hollow circular sections $I_z = I_y$ so the shape functions for bending about *z* and *y* axes have the same values.

$$\Phi_s = \frac{12EI_{si}}{L^2 G\kappa A_i}\frac{1}{C_A} \tag{72}$$

where:

s = *z* or *y* axis

Stiffness matrix coefficients

$$C_A = \begin{cases} \lim_{r_A\to 0} C_A = 1 & \Gamma=0 \\ \dfrac{r_A}{\ln(1+r_A)} & \Gamma=1 \\ (1+r_A) & \Gamma=2 \end{cases} \tag{73}$$

$$C_J = \frac{(\Gamma_J-1)r_A}{(1-(1+r_A)^{(1-\Gamma_J)})} \tag{74}$$

$$C_{Ms}=\frac{\left(1-(1+r_A)^{(1-\bar{\Gamma})}\right)}{(\bar{\Gamma}-1)r_A} \tag{75}$$

$$C_{Fs}=\frac{2}{(\bar{\Gamma}-2)r_A}\left(C_{Ms}-\frac{1}{(1+r_A)^{(\bar{\Gamma}-1)}}\right) \tag{76}$$

$$p_s=\frac{6}{(\bar{\Gamma}-2)(\bar{\Gamma}-3){r_A}^2}\left(C_{Ms}-\frac{2+(\bar{\Gamma}-2)r_A}{2(1+r_A)^{(\bar{\Gamma}-1)}}\right) \tag{77}$$

Consistent mass matrix coefficients

$$C_p=\frac{(\Gamma_p-1)r_A}{\left(1-(1+r_A)^{(1-\Gamma_p)}\right)} \tag{78}$$

The general equation that presents the elements of the consistent mass matrix for translational moment of inertia is calculated as:

$$m'_{fkl}=\rho A_i\int_0^L N_{fk}(x)\,N_{fl}(x)\left(1+r_A\frac{x}{L}\right)^{\Gamma}dx=\rho A_i\int_1^{(1+r_h)} N_{fk}(\xi_h)\,N_{fl}(\xi_h)\xi_h^{\Gamma}\left(\frac{L}{r_A}\right)d\xi_h \tag{79}$$

$$m'_{fkl}=\frac{\rho A_i L}{C_{Bs}^2}[I_{f1}+I_{f2}+I_{f3}+I_{f4}],\ k \text{ and } l=1,\ 2,\ 3,\ 4 \tag{80}$$

where:

$$I_{f1}=\left(\frac{L}{r_A}\right)^2\left[\frac{(A_{sk}B_{sl}+A_{sl}B_{sk})}{(\bar{\Gamma}-2)^2(\bar{\Gamma}-3)(\bar{\Gamma}-1)}\frac{\left((1+r_A)^{\left(6-(2\bar{\Gamma}-\Gamma)\right)}-1\right)}{\left(6-(2\bar{\Gamma}-\Gamma)\right)r_A}\right.$$
$$\left.+\frac{A_{sk}A_{sl}}{(\bar{\Gamma}-2)^2(\bar{\Gamma}-3)^2}\frac{\left((1+r_A)^{\left(7-(2\bar{\Gamma}-\Gamma)\right)}-1\right)}{\left(7-(2\bar{\Gamma}-\Gamma)\right)r_A}+\frac{B_{sk}B_{sl}}{(\bar{\Gamma}-2)^2(\bar{\Gamma}-1)^2}\frac{\left((1+r_A)^{\left(5-(2\bar{\Gamma}-\Gamma)\right)}\right.}{\left(5-(2\bar{\Gamma}-\Gamma)\right)r} \tag{81}$$

$$I_{f2}=\left(\frac{L}{r_A}\right)^2\left[\frac{C_{sk}C_{sl}}{(\bar{\Gamma}-2)^2(\bar{\Gamma}-1)^2}\frac{\left((1+r_A)^{(3+\Gamma)}-1\right)}{(3+\Gamma)r_A}+\frac{(C_{sk}E_{sl}+C_{sl}E_{sk})}{(\bar{\Gamma}-2)(\bar{\Gamma}-1)}\frac{\left((1+r_A)^{(2+\Gamma)}-1\right)}{(2+\Gamma)r_A}\right.$$
$$\left.+E_{sk}E_{sl}\frac{\left((1+r_A)^{(1+\Gamma)}-1\right)}{(1+\Gamma)r_A}\right] \tag{82}$$

$$I_{f3}=-\left(\frac{L}{r_A}\right)^2\left[\left(\frac{(A_{sk}E_{sl}+A_{sl}E_{sk})}{(\bar{\Gamma}-2)(\bar{\Gamma}-3)}+\frac{(B_{sk}C_{sl}+B_{sl}C_{sk})}{(\bar{\Gamma}-2)^2(\bar{\Gamma}-1)^2}\right)\frac{\left((1+r_A)^{(4-(\bar{\Gamma}-\Gamma))}-1\right)}{\left(4-(\bar{\Gamma}-\Gamma)\right)r_A}\right.$$
$$+\frac{(A_{sk}C_{sl}+A_{sl}C_{sk})}{(\bar{\Gamma}-2)^2(\bar{\Gamma}-3)(\bar{\Gamma}-1)}\frac{\left((1+r_A)^{(5-(\bar{\Gamma}-\Gamma))}-1\right)}{\left(5-(\bar{\Gamma}-\Gamma)\right)r_A}+\frac{(B_{sk}E_{sl}+B_{sl}E_{sk})}{(\bar{\Gamma}-2)(\bar{\Gamma}-1)}\frac{\left((1+r_A)^{(3-(\bar{\Gamma}-\Gamma))}-1\right)}{\left(3-(\bar{\Gamma}-\Gamma)\right)r_A} \quad (83)$$

$$I_{f4}=\left(\frac{L}{r_A}\right)^2\left[\frac{(D_{sk}E_{sl}+D_{sl}E_{sk})}{(\Gamma-1)}\frac{((1+r_A)^2-1)}{2r_A}+\frac{D_{sk}D_{sl}}{(\Gamma-1)^2}\frac{((1+r_A)^{(3-\Gamma)}-1)}{(3-\Gamma)r_A}\right.$$
$$+\frac{(C_{sk}D_{sl}+C_{sl}D_{sk})}{(\bar{\Gamma}-2)(\bar{\Gamma}-1)(\Gamma-1)}\frac{((1+r_A)^3-1)}{3r_A}-\frac{(B_{sk}D_{sl}+B_{sl}D_{sk})}{(\bar{\Gamma}-2)(\bar{\Gamma}-1)(\Gamma-1)}\frac{\left((1+r_A)^{(4-\bar{\Gamma})}-1\right)}{(4-\bar{\Gamma})r_A} \quad (84)$$
$$\left.-\frac{(A_{sk}D_{sl}+A_{sl}D_{sk})}{(\bar{\Gamma}-2)(\bar{\Gamma}-3)(\Gamma-1)}\frac{\left((1+r_A)^{(5-\bar{\Gamma})}-1\right)}{(5-\bar{\Gamma})r_A}\right]$$

The general equation that presents the elements of the consistent mass matrix for rotatory moment of inertia about *z* and *y* axis are calculated as:

$$m'_{\theta skl}=\rho I_{si}\int_0^L N_{\theta sk}(x)\,N_{\theta sl}(x)\left(1+r_A\frac{x}{L}\right)^{\bar{\Gamma}}dx=\rho I_{si}\int_1^{(1+r_h)} N_{\theta sk}(\xi_h)\,N_{\theta sl}(\xi_h)\xi_h^{\bar{\Gamma}}\left(\frac{L}{r_A}\right)d\xi_h \quad (85)$$

$$m'_{\theta skl}=\frac{\rho A_i L}{C_{Bs}^2}\left(\frac{r_{Gsi}}{L}\right)^2[I_{\theta s1}+I_{\theta s2}],\ k \text{ and } l=1,2,3,4 \quad (86)$$

where:

r_{Gsi}: is the radius of gyration at the start node *i* and can be performed as:

$$r_{Gsi}=\sqrt{\frac{I_{si}}{A_i}} \quad (87)$$

$$I_{\theta s1}=L^2\left[\frac{A_{sk}A_{sl}}{(\bar{\Gamma}-2)^2}\frac{((1+r_A)^{(5-\bar{\Gamma})}-1)}{(5-\bar{\Gamma})r_A}+\frac{B_{sk}B_{sl}}{(\bar{\Gamma}-1)^2}\frac{((1+r_A)^{(3-\bar{\Gamma})}-1)}{(3-\bar{\Gamma})r_A}\right.$$
$$\left.+\frac{(A_{sk}B_{sl}+A_{sl}B_{sk})}{(\bar{\Gamma}-2)(\bar{\Gamma}-1)}\frac{\left((1+r_A)^{(4-\bar{\Gamma})}-1\right)}{(4-\bar{\Gamma})r_A}\right] \quad (88)$$

$$I_{\theta s2}=L^2\left[\frac{(A_{sk}C_{sl}+A_{sl}C_{sk})}{(\bar{\Gamma}-2)^2(\bar{\Gamma}-1)}\frac{\left((1+r_A)^3-1\right)}{3r_A}+\frac{(B_{sk}C_{sl}+B_{sl}C_{sk})}{(\bar{\Gamma}-2)(\bar{\Gamma}-1)^2}\frac{\left((1+r_A)^2-1\right)}{2r_A}\right.$$

$$\left.+\frac{C_{sk}C_{sl}}{(\bar{\Gamma}-2)^2(\bar{\Gamma}-1)^2}\frac{\left((1+r_A)^{(\bar{\Gamma}+1)}-1\right)}{(\bar{\Gamma}+1)r_A}\right] \tag{89}$$

Geometric stiffness matrix coefficients

$$C_{gA}=\begin{cases}\lim\limits_{r_A\to 0} C_{gA}=1 & \Gamma=0\\ \dfrac{C_A^2}{(1+r_A)} & \Gamma=1\\ C_A^2\dfrac{\left(1-(1+r_A)^{-3}\right)}{3r_A} & \Gamma=2\end{cases} \tag{90}$$

$$C_{gT}=C_J^2\frac{\left(1-(1+r_A)^{\left(1-(2\Gamma_J-\Gamma_p+\Gamma)\right)}\right)}{r_A\left((2\Gamma_J-\Gamma_p+\Gamma)-1\right)} \tag{91}$$

The general equation that presents the elements of geometric stiffness matrix is:

$$k'_{gfkl}=F_{xi}\int_0^L N'_{fk}(x)\,N'_{fl}(x)dx=F_{xi}\int_1^{(1+r_h)} N'_{fk}(\xi_h)\,N'_{fl}(\xi_h)\left(\frac{L}{r_A}\right)d\xi_h \tag{92}$$

$$k'_{gfkl}=\frac{F_{xi}}{C_{Bs}^2L}\left[I_{gf1}+I_{gf2}+I_{gf3}\right],\ k \text{ and } l=1,\ 2,\ 3,\ 4 \tag{93}$$

where:

$$I_{gf1}=L^2\left[\frac{A_{sk}A_{sl}}{(\bar{\Gamma}-2)^2}\frac{\left((1+r_A)^{(5-2\bar{\Gamma})}-1\right)}{(5-2\bar{\Gamma})r_A}+\frac{(A_{sk}B_{sl}+A_{sl}B_{sk})}{(\bar{\Gamma}-2)(\bar{\Gamma}-1)}\frac{\left((1+r_A)^{(4-2\bar{\Gamma})}-1\right)}{(4-2\bar{\Gamma})r_A}\right.$$

$$\left.+\frac{B_{sk}B_{sl}}{(\bar{\Gamma}-1)^2}\frac{\left((1+r_A)^{(3-2\bar{\Gamma})}-1\right)}{(3-2\bar{\Gamma})r_A}\right] \tag{94}$$

$$I_{gf2}=L^2\left[\frac{(A_{sk}C_{sl}+A_{sl}C_{sk})}{(\bar{\Gamma}-2)^2(\bar{\Gamma}-1)}\frac{\left((1+r_A)^{(3-\bar{\Gamma})}-1\right)}{(3-\bar{\Gamma})r_A}+\frac{(B_{sk}C_{sl}+B_{sl}C_{sk})}{(\bar{\Gamma}-2)(\bar{\Gamma}-1)^2}\frac{\left((1+r_A)^{(2-\bar{\Gamma})}-1\right)}{(2-\bar{\Gamma})r_A}+\frac{C_{sk}C_{sl}}{(\bar{\Gamma}-2)^2(\bar{\Gamma}-1)^2}\frac{\left((1+r_A)-1\right)}{r_A}\right] \tag{95}$$

$$I_{gf3}=L^2\left[-\frac{(A_{sk}D_{sl}+A_{sl}D_{sk})}{(\bar{\Gamma}-2)}\frac{\left((1+r_A)^{\left(3-(\bar{\Gamma}+\Gamma)\right)}-1\right)}{\left(3-(\bar{\Gamma}+\Gamma)\right)r_A}-\frac{(B_{sk}D_{sl}+B_{sl}D_{sk})}{(\bar{\Gamma}-1)}\frac{\left((1+r_A)^{\left(2-(\bar{\Gamma}+\Gamma\right.}\right.}{\left(2-(\bar{\Gamma}+\Gamma)\right)}-\frac{(C_{sk}D_{sl}+C_{sl}D_{sk})}{(\bar{\Gamma}-2)(\bar{\Gamma}-1)}\frac{\left((1+r_A)^{(1-\Gamma)}-1\right)}{(1-\Gamma)r_A}+D_{sk}D_{sl}\frac{\left((1+r_A)^{(1-2\Gamma)}-1\right)}{(1-2\Gamma)r_A}\Bigg] \tag{96}$$

REFERENCES

1. *Aissa, M., Bouzid, D., Bhattacharya, S.* (2018): "Monopile head stiffness for serviceability limit state calculations in assessing the natural frequency of offshore wind turbines", International Journal of Geotechnical Engineering, Vol. 12, No. 3, 267-283.

2. *Álamo, G. etc al.* (2018): "Dynamic soil-structure interaction in offshore wind turbines on monopiles in layered seabed based on real data", Ocean Engineering, Volume 156, Pages 14-24.

3. *Arany, L. etc al.* (2015): " An analytical model to predict the natural frequency of offshore wind turbines on three-spring flexible foundations using two different beam models", Soil Dynamics and Earthquake Engineering, Volume 74, Pages 40-45.

4. *Arany, L. etc al.* (2016): "Closed form solution of Eigen frequency of monopile supported offshore wind turbines in deeper waters incorporating stiffness of substructure and SSI", Soil Dynamics and Earthquake Engineering Volume 83, Pages 18-32.

5. *Attarnejad, R., Semnani, Sh. J.* and *Shahba, A.* (2010): "Basic displacement functions for free vibration analysis of non-prismatic Timoshenko beams", Finite Element in Analysis and Design, 46(2010), 916-929.

6. *Bai, R.*, *Liu*, *S.* and *Chan*, *S.* (2018): "Finite-element implementation for nonlinear static and dynamic frame analysis of tapered members", Engineering Structures 172 (2018), 358-381.

7. *Bai, R.*, *Liu*, *S.* and *Chan*, *S.* (2018): "Modal and time-history analysis of frames with tapered sections by non-prismatic elements", International Journal of Structural Stability and Dynamics, Vol. 18, No. 9 (2018) 1850106 (34 pages).

8. *Bhattacharya, S.* (2019): "Design of Foundations for Offshore Wind Turbines", John Wiley & Sons Ltd, UK.

9. *Bottega, W.* (2006): "Engineering Vibrations", 2nd edition, CRC Press, New York, USA.

10. *Bower, A.* (2010):" Applied Mechanics of Solids" CRC Press, New York, USA.

11. *Chalah F., Chalah-Rezgui L., Djellab S.E., Bali A.* (2020): "Axial Fundamental Vibration Frequency of a Tapered Rod with a Linear Cross-Sectional Area Variation" In: Öchsner A., Altenbach H. (eds) Engineering Design Applications III. Advanced Structured Materials, vol 124. Springer, Cham.

12. *Chopra, A.* (2020): "Dynamics of Structures: Theory and Applications to Earthquake Engineering", 5th edition, Pearson Education Limited, United Kingdom.

13. *Cowper, G. R.* (1966): "The shear coefficient in Timoshenko's beam theory.", J. Appl. Mech., 33(2), 335–340.

14. *Darvishi-Alamouti, S., Bahaari, M.R., Moradi, M.* (2017): "Natural frequency of offshore wind turbines on rigid and flexible monopiles in cohesionless soils with linear stiffness distribution", Applied Ocean Research, Volume 68, Pages 91-102.

15. *Edenhofer O. et al*. (2012): IPCC Special Report on Renewable Energy Sources and Climate Change Mitigation, (Cambridge University Press).

16. *Ghali, A.,* and *Neville, A. M.* (2017): "Structural Analysis: A unified classical and matrix approach", 7th edition, CRC Press, LLC, Florida, USA.

17. http://www.wind-power-program.com/UK_wind_speed_database.htm

18. https://rechneronline.de/pi/truncated-cone.php

19. https://www.wolframalpha.com/calculators

20. *Hu, Y., Baniotopoulos, C., Yang, J.* (2014): "Effect of internal stiffening rings and wall thickness on the structural response of steel wind turbine towers", Engineering Structures, 81, 148–161.

21. *Humar, J.* (2012): "Dynamics of Structures", 3rd edition, CRC press, Taylor and Francis Group, New York.

22. *Hutchinson, J. R.* (2001): "Shear coefficients for Timoshenko beam theory.", J. Appl. Mech., 68(1), 87–92.

23. *Kim, T., Park, I., and Lee, U.* (2017):"Forced Vibration of a Timoshenko Beam Subjected to Stationary and Moving Loads Using the Modal Analysis Method", Shock and Vibration 2017(5):1-26.

24. *Letcher, T.* (2017): "Wind Energy Engineering: A Handbook for Onshore and Offshore Wind Turbines", Academic Press, Elsevier Inc., UK.

25. *Logan, D.* (2012): "A First Course in the Finite Element Method", 5th Edition, Boston, MA: Cengage Learning, the USA.

26. *Logan, D.* (2012): "Instructor's Solution's Manual to Accompany A First Course in the Finite Element Method" 5th Edition, Boston, MA: Cengage Learning, the USA.

27. *Lou P., Dai G-L., and Zeng Q-Y*. (2006): "Finite-Element Analysis of *Timoshenko* Beam Subjected to a Moving mass", Proc. IMechE Vol. 220 Part C: J. Mechanical Engineering Science.

28. *McGuire, W., Gallagher, H., Ziemian, R.* (1999): "Matrix Structural Analysis", 2nd Edition, John Wiley & Sons, Inc., New York, USA.

29. *Navadeh, N., Hewson, R.W.* and *Fallah, A.S.* (2018): "Dynamics of transversally vibrating non-prismatic Timoshenko Cantilever beams", Engineering structures, 166 (2018), 511-525.

30. *Rose K. G.* (2017): "Computational Methods for Nonlinear Systems Analysis with Applications in Mathematics and Engineering", PhD Thesis, ODU Digital Commons, Mechanical & Aerospace Engineering Theses & Dissertations.

31. *Ross, C. T. F.* (1998): "Advanced Finite Element Methods", Horwood publishing limited, Chichester, UK.

32. *Sewell, D. etc al.* (2012): "Incorporation of Multi-Member Substructure Capabilities in FAST for Analysis of Offshore Wind Turbines", Conference Paper NREL/CP-5000-53676, May 2012.

33. *Soltani, M.*, *Asgarian, B.* (2018): "Finite element formulation for linear stability analysis of axially functionally graded non-prismatic *Timoshenko* beam, International Journal of Structural Stability and Dynamics.

34. *Tudjono, S., etc al* (2017):"Exact shape functions for Timoshenko beam element", IOSR-JCE, Volume 19, Issue 3, 12-20.

35. *Wang, C.M., Wang, C. Y.* and *Reddy, J. N.* (2005): "Exact solutions for Buckling of structural members", CRC Press, LLC, Florida, USA.

36. *Yang, Y.* and *Kang, J.* (2018): "Closed-form exact solutions for hysteretically damped longitudinal free and forced vibrations of tapered beams", Acta Mech. 229, 4741-4751.

37. *Yokoyama, T*. (1996): "Vibration analysis of *Timoshenko* beam-columns on two parameter elastic foundations. Comput. Struct., 1996, 61(6), 995-1007.

38. *Yung-Yen Ko* (2020): "A Simplified structural model for monopile-supported offshore wind turbines with tapered towers", Renewable Energy, 156, 77-790.